

# A fluorescent sphingolipid binding domain peptide probe interacts with sphingolipids and cholesterol-dependent raft domains<sup>§</sup>

Sarita Hebbar,<sup>\*</sup> Esther Lee,<sup>\*</sup> Manoj Manna,<sup>\*,†</sup> Steffen Steinert,<sup>1,\*</sup> Goparaju Sravan Kumar,<sup>2,§</sup> Markus Wenk,<sup>§</sup> Thorsten Wohland,<sup>†</sup> and Rachel Kraut<sup>3,\*</sup>

Institute of Bioengineering and Nanotechnology,<sup>\*</sup> The Nanos, Singapore 138669; and Department of Chemistry,<sup>†</sup> and Department of Biochemistry,<sup>§</sup> National University of Singapore, Singapore

**Abstract** We have designed a tagged probe [sphingolipid binding domain (SBD)] to facilitate the tracking of intracellular movements of sphingolipids in living neuronal cells. SBD is a small peptide consisting of the SBD of the amyloid precursor protein. It can be conjugated to a fluorophore of choice and exogenously applied to cells, thus allowing for in vivo imaging. Here, we present evidence to describe the characteristics of the SBD association with the plasma membrane. Our experiments demonstrate that SBD binds to isolated raft fractions from human neuroblastomas and insect neuronal cells. In protein-lipid overlay experiments, SBD interacts with a subset of glycosphingolipids and sphingomyelin, consistent with its raft association in neurons. We also provide evidence that SBD is taken up by neuronal cells in a cholesterol- and sphingolipid-dependent manner via detergent-resistant microdomains. Furthermore, using fluorescence correlation spectroscopy to assay the mobility of SBD in live cells, we show that SBD's behavior at the plasma membrane is similar to that of the previously described raft marker cholera toxin B, displaying both a fast and a slow component. Our data suggest that fluorescently tagged SBD can be used to investigate the dynamic nature of glycosphingolipid-rich detergent-resistant microdomains that are cholesterol-dependent.—Hebbar, S., E. Lee, M. Manna, S. Steinert, G. S. Kumar, M. Wenk, T. Wohland, and R. Kraut. A fluorescent sphingolipid binding domain peptide probe interacts with sphingolipids and cholesterol-dependent raft domains. *J. Lipid Res.* 2008. 49: 1077–1089.

**Supplementary key words** fluorescent probe • lipid rafts • detergent-resistant microdomains • amyloid  $\beta$  peptide • fluorescence correlation spectroscopy

The involvement of cholesterol and sphingolipid-rich membrane microdomains known as lipid rafts in a variety of cellular processes is well established (reviewed in Refs. 1, 2), and raft-borne lipids and proteins have been

implicated in several pathological conditions, including neurodegeneration and inflammation (reviewed in Ref. 3). Previously, cholera toxin B (CtxB) was used to study the intracellular trafficking of raft-borne lipids (4–8). Studies on the uptake mechanisms, intracellular itineraries, and biophysical properties of raft-associated proteins at the plasma membrane have revealed heterogeneity in their trafficking and dynamic behavior (9–12). Currently, very little is known about how different ligands associate with raft domains, to what extent the lipid content in those domains differs, and what effect raft lipids have on intracellular targeting. To begin to answer these questions, it will be necessary to develop a diverse battery of markers to characterize the determinants of binding and trafficking behaviors.

Here, we present the biochemical and biophysical characterization of a novel, fluorescently tagged sphingolipid binding raft probe, the sphingolipid binding domain (SBD), derived from the amyloid  $\beta$  peptide (A $\beta$ ). This motif, identified by Fantini (13) in several glycolipid-associated proteins, was postulated to form a V3 loop structure that interacts with the sugar rings in glycosphingolipid head groups. In a separate study (S. Steinert and E. Lee, unpublished data), we showed that fluorescent SBD is targeted to endolysosomal compartments in a cholesterol-dependent manner and that it interacts with

Abbreviations: A $\beta$ , amyloid  $\beta$  peptide; c6, cell line DL-DMBG2-c6; CtxB, cholera toxin B; DiI, dialkyl-indocarbocyanine; DRM, detergent-resistant membrane; FB1, fumonisin B1; FCS, fluorescence correlation spectroscopy; GFP, green fluorescent protein; HFIP, 1,1,1,3,3,3-hexafluoro-2-propanol; M $\beta$ CD, methyl- $\beta$ -cyclodextrin; OG, Oregon green; SBD, sphingolipid binding domain; TMR, tetramethyl rhodamine.

<sup>1</sup>Present address of S. Steinert: Physikalisches Institut, Technische Universität Stuttgart, Pfaffenwaldring 5, D-70550 Stuttgart, Germany.

<sup>2</sup>Present address of G. S. Kumar: Division of Biochemistry, Department of Molecular and Cellular Biology, Kobe University Graduate School of Medicine, Kobe 650-0017, Japan.

<sup>3</sup>To whom correspondence should be addressed.

e-mail: rkraut@ibn.a-star.edu.sg

<sup>§</sup>The online version of this article (available at <http://www.jlr.org>) contains supplementary data in the form of four figures.

Manuscript received 26 November 2007 and in revised form 28 January 2008.

Published, *JLR Papers in Press*, February 8, 2008.

DOI 10.1194/jlr.M700543-JLR200

Copyright © 2008 by the American Society for Biochemistry and Molecular Biology, Inc.

This article is available online at <http://www.jlr.org>

raft-like lipid mixtures in liposome binding assays and by surface plasmon resonance.

We used standard raft isolation methods in conjunction with lipid-protein overlays, live cell imaging, and fluorescence correlation spectroscopy (FCS) to describe the characteristics of SBD association with the plasma membrane. Lipid-protein overlay experiments (fat blots) suggest that SBD interacts with particular gangliosides and sphingomyelin, which are generally thought to reside in raft domains. We also demonstrate that SBD interacts predominantly with detergent-insoluble membrane fractions isolated from neuronal cells, similar to other known raft markers. Moreover, its endocytic uptake by neurons is dependent on the presence of intact microdomains, which can be disrupted by cholesterol or sphingolipid depletion. By FCS, we demonstrate that SBD displays mobility characteristics at the plasma membrane that are consistent with partial raft association and shows a distribution of diffusion times strikingly similar to that of CtxB. Pharmacological removal of cholesterol reduced the SBD association with detergent-resistant membranes (DRMs), dependent on cell type. However, in live cell labeling, uptake at the plasma membrane was cholesterol- and sphingolipid-dependent in both neuronal types tested. In summary, we suggest that SBD can serve as a useful tool for the study of cholesterol-dependent sphingolipid membrane microdomains and their trafficking.

## METHODS

### Cell culture

The *Drosophila* neuronal cell line DL-DMBG2-c6 (c6; *Drosophila* Genome Resource Center) (14) was grown at 25°C in Shields and Sang M3 medium (Gibco) with 10% FBS (Gibco), 0.125 IU/ml bovine insulin (Biological Industries), and 1% antibiotic/antimycotic solution (Gibco). NIH 3T3 mouse fibroblasts and SH-SY5Y neuroblastoma (American Type Culture Collection-ATCC) were grown at 37°C in DMEM (Gibco) supplemented with 10% FBS and antibiotic.

One microgram of plasmid DNA was used along with Lipofectamine 2000 (Invitrogen) for transfections according to the manufacturer's instructions. Flotillin-green fluorescent protein (GFP) plasmid (a kind gift from L. Briggs and S. Sweeney) has the flotillin sequence under the control of the Act5c promoter that is constitutively active in *Drosophila* cells. For use in neuroblastomas, flotillin-GFP was cloned into pcDNA 3.1 (Invitrogen) with cytomegalovirus promoter.

For labeling of free cholesterol with filipin, cells were fixed in 4% paraformaldehyde for 3 min followed by washes in HBSS/HEPES. Cells were incubated with 50 µg/ml filipin (Sigma) for 45 min and then washed before imaging.

### SBD peptide handling and cell labeling

SBD peptide linked to an N-terminal cysteine and an inert spacer (cysteine-amino-ethoxy-ethoxy-acetyl[AEEAc]2-DAEFRH-DSGYEVHHQELVFFAEDVG), thiol-coupled with Oregon green (OG) or amine-coupled with tetramethyl rhodamine (TMR) directly to the spacer, was synthesized by Bachem. Myc-tagged SBD was synthesized by GenScript Corp. A mutated sequence (DAEFA-HDSGAEVHHQELVFFAEDVG) and a scrambled sequence (FY-

HDESEFGHAVEQFGRDVEAVHDL) were also coupled to myc as controls. To avoid aggregate formation of the peptide, SBD was dissolved in 1,1,1,3,3,3-hexafluoro-2-propanol (HFIP; Merck), divided into aliquots, and dried. For larger volumes of peptide, evaporation was done under a supply of inert nitrogen. Lyophilized peptide was stored at -20°C and redissolved in DMSO immediately before use. Peptide was diluted to a final working concentration of 10 µM in HBSS (Gibco), supplemented with 10 mM HEPES, incubated at 25°C for 30 min at 10 µM (for *Drosophila* cells) or at 37°C at 5 µM (for mammalian cells), and then washed three times in HBSS. For lipid overlays/fat blot experiments, the peptide film obtained after HFIP evaporation was dissolved in DMSO and then in Tris buffer, pH 7.4 (the final concentration of DMSO in buffer did not exceed 1%).

### Drug treatments

For cholesterol depletion, cells were incubated in 10 mM methyl-β-cyclodextrin (MβCD; Sigma) for 30 min (in serum-free medium for c6 cells or in medium supplemented with 1% FBS for neuroblastomas) and washed. The Amplex Red Cholesterol Assay kit (Invitrogen) was used to measure cholesterol concentrations in cell extracts before OptiPrep gradient formation and later on the DRM fractions generated.

For sphingolipid depletion, cells were incubated with 10 µM fumonisin B1 (FB1; AG Scientific F1022) for 2 h at 37°C, washed three times with HBSS/HEPES before being labeled with transferrin 594 (Molecular Probes) or CtxB 594 (Molecular Probes) at 37°C for 30 min, and then washed three times with HBSS/HEPES before being imaged in phenol red-free DMEM/F12 with FB1 (10 µM).

### Isolation of DRM fractions

DRMs were isolated as described by Zhai, Chaturvedi, and Cumberledge (15). Briefly, cells from a confluent plate were washed with phosphate-buffered saline and then resuspended in 0.8 ml of TNET lysis buffer (100 mM Tris, pH 7.5, 20 mM EGTA, 150 mM NaCl, 1% Triton X-100, and protease inhibitor cocktail; Sigma). The postnuclear supernatant was diluted 1:2 with 60% OptiPrep (Accurate Chemicals and Scientific Corp.). Cell lysate-OptiPrep solution was overlaid with 7.2 ml of 30% and 2.4 ml of 5% OptiPrep solution in a Beckman SW41 tube and centrifuged at 41,000 rpm for 5 h at 4°C. Twelve fractions of 1 ml were collected from the top of the gradient and subjected to routine SDS-PAGE or dot blot analysis.

### Immunoblotting

For the lipid-protein overlay assay, Sphingotrips (Invitrogen) were used according to the manufacturers' instructions and protocol as described (16). Additional sphingolipids (GM1, galactocerebrosides, sphingomyelin, GD1a, GD1b, GT1b, phosphoethanolamine ceramide; Sigma) were spotted onto Hybond C nitrocellulose strips (Amersham) and allowed to dry. These strips were then exposed to 5–20 µM peptides. For dot blots, equal volumes of each fraction were blotted onto nitrocellulose membrane and exposed to antibodies against various raft and nonraft proteins, or 5–10 µM peptide solution in PBST or 1 ng/ml peroxidase-conjugated CtxB (Invitrogen) or 1 µg/ml Lysenin (Peptide Institute).

The following primary antibodies were used: 8C3 (anti-syntaxin; Developmental Studies Hybridoma Bank); 9E10 (HRP-conjugated, 1:200; Santa Cruz); anti-caveolin (1:1,000; BD Pharmingen); anti-flotillin (1:1,000; Transduction Laboratories); anti-Lysenin (1:1,000; Peptide Institute); and anti-rac (1:250; BD Pharmingen). Primary antibody treatment was followed by

peroxidase-conjugated secondary antibody exposure, and then blots were developed using standard chemiluminescent detection (Amersham). Intensity quantification from dot blots was carried out using Quantity-One (Bio-Rad Laboratories) software.

### Imaging and FCS

For uptake experiments, images were acquired with a Cool-snapHQ charged coupled device camera on a Deltavision (Applied Precision) wide-field microscope with a 60×/1.42 numerical aperture oil lens (Olympus) and a standard filter set (green: excitation, 490/20, emission, 528/38; red: excitation, 555/28, emission 617/73) (Chroma). Quantification of images was performed using the MetaMorph image-processing program as described previously (17). Whole cell fluorescence was determined by drawing borders around individual cells, and noncellular background was subtracted. All photomicrographs in a given experiment were exposed and processed identically for a given fluorophore.

The FCS instrumental setup used in this study is an Olympus FV300 confocal microscope, with which correlator and Avalanche photo detectors are coupled in house. To excite BODIPY-FL-SM and SBD-OG, a 488 nm argon laser was used, and the emission signal was detected through a 510 AF23 emission filter. Dialkylindocarbocyanine (DiI), CtxB-Alexa-594, and TMR-SBD were excited with a 543 nm He-Ni laser and were detected through a 595 AF60 emission filter. For all measurements, 100 μW laser power before the microscope objective was used. The measurement was carried out as follows: a cell was first imaged in transmitted light, using the XY scan of the Fluoview software of the Olympus confocal system, followed by choosing a region of interest by adjusting the proper Z plane and then performing FCS in the fluorescence point scanning mode. The Avalanche photo detector creates an intensity plot of the fluorescence signal from the sample, and the hardware correlator calculates the autocorrelation function,  $G(\tau)$ , expressed as  $\{[\delta F(t) \delta F(t+\tau)]/[F(t)]^2\}$ , where  $F(t)$  is the fluorescence fluctuation caused by a particle at time  $t$  and  $F(t+\tau)$  is for the same particle at time point  $(t+\tau)$  (18, 19). Igor Pro software (version 4) was used to fit the data to the FCS curve-fitting model. The equations for the  $G(\tau)$  fitting models used are as follows:

2D1P1t:

$$G(\tau) = \frac{1}{N} \times \left[ \left\{ \frac{1}{(1 + \tau/\tau_D)} \right\} \left\{ 1 + \frac{F_{\text{trip}}}{(1 - F_{\text{trip}})} \times e^{-(\tau/\tau_{\text{trip}})} \right\} \right] + 1$$

2D2P1t:

$$G(\tau) = \frac{1}{N} \left[ \left\{ \frac{(1 - F_2)}{(1 + \tau/\tau_D)} \right\} \left\{ \frac{F_2}{(1 + \tau/\tau_{D_2})} \right\} \times \left\{ 1 + \frac{F_{\text{trip}}}{(1 - F_{\text{trip}})} \times e^{-(\tau/\tau_{\text{trip}})} \right\} \right] + 1$$

3D1P1t:

$$G(\tau) = \frac{1}{N} \left[ \left\{ \frac{(1 + \tau/\tau_D)^{-1}}{\sqrt{1 + (\tau/\tau_D)K^{-2}}} \right\} \times \left\{ 1 + \frac{F_{\text{trip}}}{(1 - F_{\text{trip}})} \times e^{-(\tau/\tau_{\text{trip}})} \right\} \right] + 1$$

3D2P1t:

$$G(\tau) = \frac{1}{N} \left[ \left\{ \frac{(1 - F_2)(1 + \tau/\tau_D)^{-1}}{\sqrt{1 + (\tau/\tau_D)K^{-2}}} \right\} \left\{ \frac{F_2 \times (1 + \tau/\tau_{D_2})^{-1}}{\sqrt{1 + (\tau/\tau_{D_2})K^{-2}}} \right\} \times \left\{ 1 + \frac{F_{\text{trip}}}{(1 - F_{\text{trip}})} \times e^{-(\tau/\tau_{\text{trip}})} \right\} \right] + 1$$

## RESULTS

### SBD binds to isolated detergent-insoluble fractions of insect and human neuronal cells

Association with DRM fractions has been used as a method to detect raft association (20). Although DRM binding by itself is insufficient to prove raft association, it is generally considered a necessary criterion. Therefore, we used SBD conjugated to a myc tag to analyze binding to DRMs isolated from different cell types that are spotted onto membranes.

Because our goal is to characterize SBD for the study of lipid trafficking in *Drosophila* and other cellular neurodegeneration models, we carried out experiments on *Drosophila* neuronal cells and mammalian neurons. It has been established that DRMs can be isolated from *Drosophila* embryonic membranes and cell lines and have similar properties to those isolated from mammalian cells (15, 21, 22). We validate the use of SBD as a raft/sphingolipid tracer by comparing its behavior in the fly neuronal cell line c6 versus SH-SY5Y neuroblastomas, which are susceptible to Aβ toxicity (23).

*Drosophila* c6 neurons and SH-SY5Y neuroblastomas were solubilized with cold 1% Triton X-100 and fractionated by high-speed centrifugation into detergent-resistant/insoluble (DRM) and nonresistant/soluble (non-DRM) membrane fractions over an OptiPrep density gradient (see Methods). These fractions were spotted onto membranes and then incubated with SBD-myc. To verify DRM isolation from c6 cells, fractions were assayed for association with a transfected known raft protein, flotillin-GFP, and an endogenous nonraft protein, rac, by Western and dot blots. In c6 cells, flotillin is broadly distributed over DRM fractions; it is present in fraction 3 and somewhat more enriched in fractions 4 and 5 (Fig. 1A). In contrast, the nonraft protein rac (15) is excluded from fractions 3 and 4 and is found primarily in the more soluble bottom fractions 9 and 10 (Fig. 1A). We also used the binding of another raft marker, GM1, to bind CtxB to isolated fractions as an additional criterion for rafts. CtxB binds most prominently to fraction 3 and to a lesser extent to fractions 1 and 2 (Fig. 1B). Therefore, based on the above four criteria (detergent resistance on a density gradient, presence of flotillin, binding of CtxB, and the exclusion of rac), we define fraction 3 as diagnostic for DRM/raft association in our assay (Fig. 1). By the same dot blot assay, SBD was seen to bind strongly to raft fraction 3, to a lesser extent to fractions 2 and 4, and also to the more soluble fractions 10 and 11 (Fig. 1B).

In the neuroblastomas, the raft protein flotillin partitioned preferentially into fractions 3 and 4 and to the more soluble fractions 11 and 12 (Fig. 1C). This dual distribution was even more pronounced on the dot blots (Fig. 1D). The other raft marker, CtxB, also displayed interactions with fractions 1–4 from the top of the gradient and with the more soluble fractions 10 and 11 (Fig. 1D). That CtxB profiles are different for the two cell types may be attributable to CtxB binding to different target lipids in fly versus human neurons. Flies do not



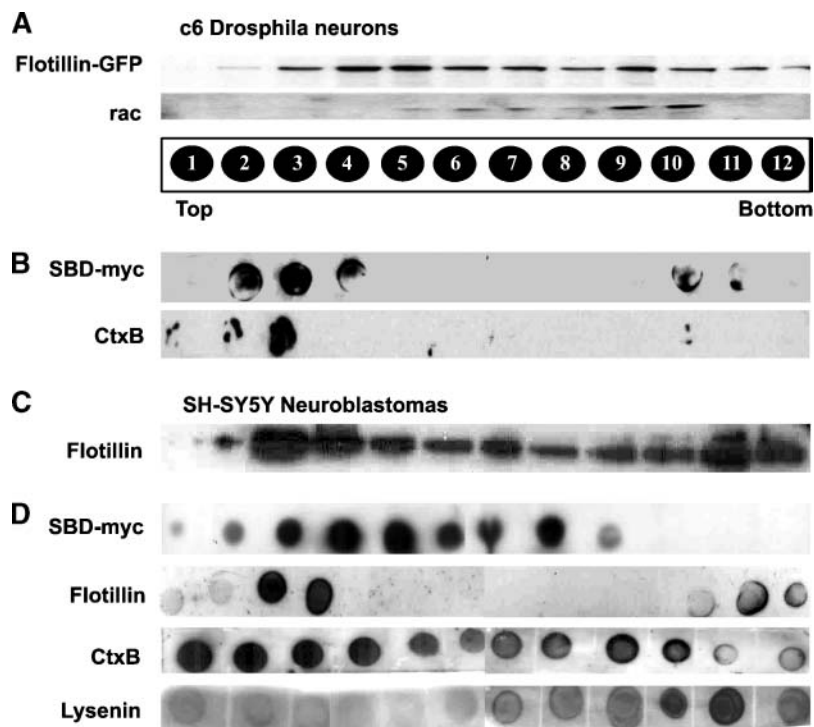


**Fig. 1.** Detergent-resistant membranes (DRMs) isolated from *Drosophila* cell line DL-DMBG2-c6 (c6) neurons interact with sphingolipid binding domain (SBD) and other raft markers. **A:** DRM fractions [DRMs 1 (top; detergent-insoluble) to 12 (bottom; detergent-soluble)] from *Drosophila* c6 neuronal cells [transfected with the raft marker flotillin-green fluorescent protein (GFP)] were isolated on OptiPrep density gradients. Fractions were characterized for the presence of flotillin and the nonraft marker rac using SDS-PAGE and Western blotting. **B:** Fractions were blotted onto a nitrocellulose membrane and exposed to SBD conjugated to myc (SBD-myc) and cholera toxin B (CtxB). SBD binds to the detergent-resistant fractions 2–4 (C) isolated from c6 cells. It also binds to less dense fractions (10 and 11). CtxB binds to fractions 2 and 3. **C:** DRM fractions from human neuroblastomas, SH-SY5Y, were isolated as described above. As a control, fractions were assayed for the presence of a raft marker, flotillin, using SDS-PAGE and Western blotting. **D:** The same fractions used above were blotted onto a nitrocellulose membrane and incubated with SBD-myc, antibody to flotillin, GM1 binding CtxB, and Lysenin. In a profile similar to that of CtxB but in contrast to that of Lysenin, SBD binds primarily to more buoyant, detergent-resistant fractions (3 and 4) but also to intermediate density fractions (5–8).

make GM1, the target of CtxB in mammalian cells (24), but they do have terminal galactose-bearing glycolipids that could interact weakly with CtxB. From flotillin distribution patterns and CtxB binding, we conclude that there has been a separation of DRMs in fractions 3 and 4. Using the dot blot assay, SBD was seen to bind strongly to DRM fractions 3 and 4 (Fig. 1D) in addition to its binding to fractions 5–8. We note that sphingomyelin binding Lysenin (11, 25), which was used as an additional standard because sphingomyelin is expected to be at least partially raft-localized (26, 27), bound to non-DRM fractions of neuroblastomas (Fig. 1D). This does not, however, contradict published data on Lysenin, because its association with DRMs per se has not been reported.

#### The DRM association of SBD is abrogated by cholesterol depletion in a cell type-dependent manner

Next, we examined whether SBD interacts with domains on intact cells that can later be isolated into DRM fractions (Fig. 2). Cells were incubated with SBD-myc, and subsequently, DRM fractions were isolated and ex-

amined for the presence of known raft markers and SBD. Enrichment of cholesterol (Fig. 2A), the distribution of raft markers such as flotillin (Fig. 2B) and caveolin (Fig. 2E), binding to CtxB (Fig. 2C), and the distribution of the nonraft protein rac indicate successful isolation of DRMs. Based on these criteria, we define fractions 2–4 in c6 cells and fractions 1–4 in neuroblastomas to include DRMs. In both *Drosophila* c6 cells and neuroblastomas, SBD is taken up in DRM fractions in addition to being taken up in more soluble fractions (Fig. 2D). Its association with non-DRM fractions is not unusual among bona fide raft markers (e.g., syntaxin in *Drosophila* membranes, which also follows a broad distribution along the density gradient) (15). In contrast to the neuronal cell types, SBD did not show a strong preference for uptake via DRM fractions of mammalian NIH 3T3 fibroblasts, segregating roughly equally between the caveolin-positive “raft” fractions (4–6) and the rac-positive “nonraft” fractions (7–12) (Fig. 2E).

Treatments that inhibit cholesterol synthesis or that remove cholesterol from membranes are known to disrupt lipid rafts. Therefore, we used M $\beta$ CD to deplete c6 and

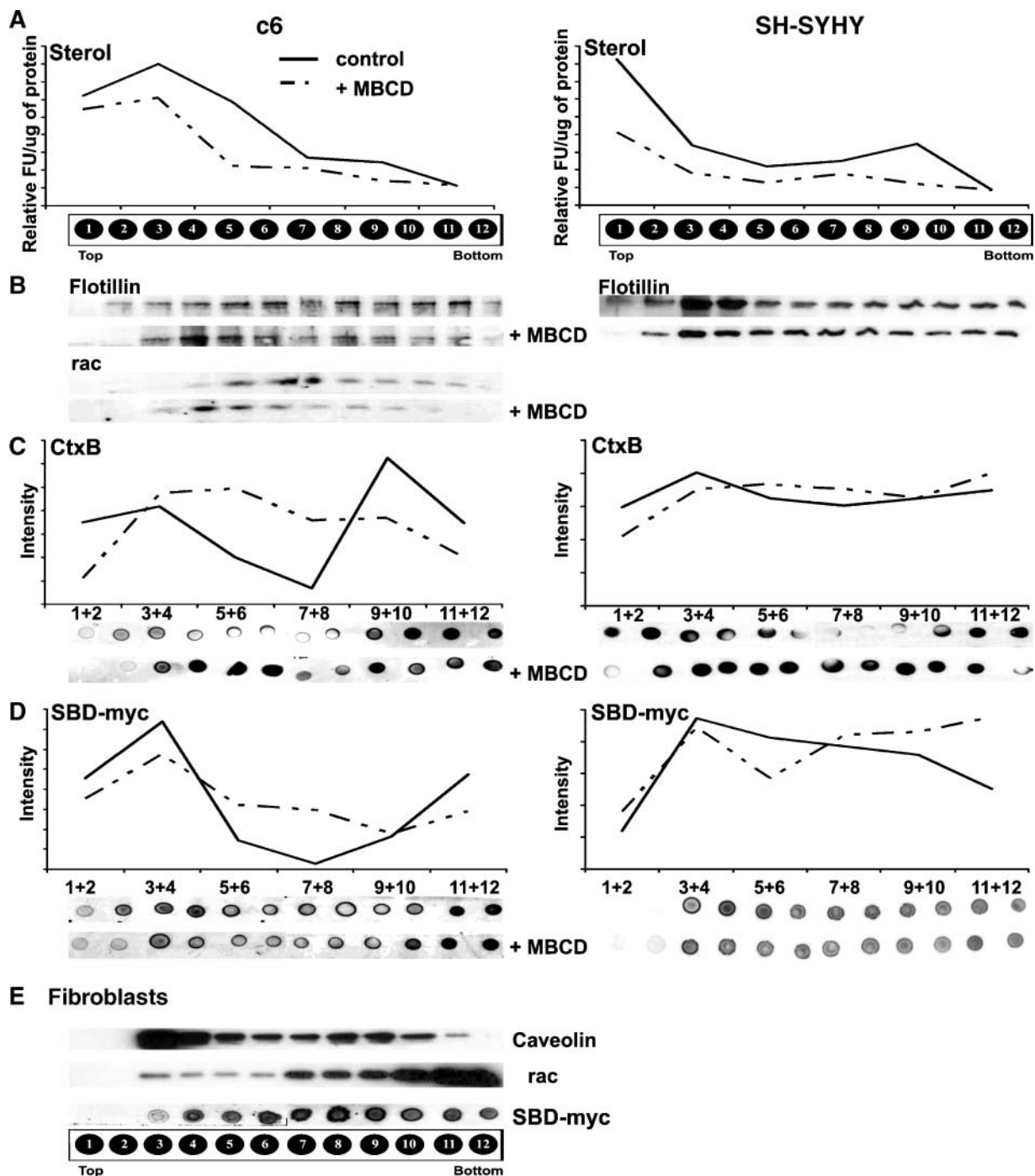


**Fig. 2.** SBD associates with cholesterol-containing domains of neuronal cells that can be isolated in DRMs. c6 cells (left panels), SH-SY5Y neuroblastomas (right panels), and NIH 3T3 fibroblasts (E) were incubated with SBD-myc for 30 min and then detergent-resistant fractions [fractions 1 (top) to 12 (bottom)] were isolated. Fractions 1–12 were examined for their sterol content (A) and for the distribution of the raft marker flotillin, caveolin (for fibroblasts), and the nonraft marker rac (Western blots; B, E). Fractions 1–12 were blotted onto a membrane and examined for interaction with CtxB (C) and myc immunoreactivity to detect SBD (D). SH-SY5Y and c6 cells were also treated with 10 mM methyl- $\beta$ -cyclodextrin (M $\beta$ CD) to deplete cells of cholesterol. In the graphs, dashed lines represent cells treated with M $\beta$ CD and solid lines represent untreated (control) cells. Line profiles in A depict relative sterol levels measured as fluorescence levels normalized to protein content. Line profiles in C and D depict the relative abundance of SBD-myc (D) and the binding of CtxB (C) in isolated fractions, both measured as intensity of dot blots and combined for successive fractions. In nontreated controls of both neuronal cell types, there is an enrichment of sterols in detergent-insoluble fractions (1–3 for neuroblastomas and 1–6 for c6 cells). Treated cell fractions (dashed) show substantial cholesterol reduction at the top of the gradient compared with the bottom of the gradient. Cholesterol depletion reduced CtxB's interaction with detergent-insoluble fractions in SH-SY5Y neuroblastomas (fractions 1 and 2) and in c6 cells (fractions 1 and 2). In c6 cells (D), fractionation of SBD-myc in DRM fractions 2 and 4 is reduced upon cholesterol depletion. In neuroblastomas, SBD uptake into detergent-resistant fraction 4 appears to be reduced. Detergent-resistant fractions of NIH 3T3 fibroblasts (E) are enriched for lipid raft markers such as caveolin (fractions 3–7) but not for nonraft markers such as rac. SBD is not preferentially taken up into detergent-insoluble fractions of fibroblasts. FU, fluorescence units.

neuroblastoma cells of cholesterol and related sterols (see Methods) and looked at the effect on SBD internalization. First, we tested the effectiveness of the M $\beta$ CD treatment by measuring total cholesterol levels using the Amplex Red Cholesterol Assay method (Invitrogen). On c6 cells, cholesterol was reduced by  $46.7 \pm 7.8\%$  (average of two experiments) after 30 min, and in the neuroblastomas, we observed a reduction of  $51.8 \pm 8.4\%$  (average of two experiments). We also examined the sterol levels across the fractions obtained by density centrifugation (Fig. 2A, line profiles). In both cell types used, M $\beta$ CD treatment causes the distribution of the remaining cholesterol to become more uniform across the density gradient (Fig. 2A). Also, M $\beta$ CD treatment results in a larger depletion of cholesterol from the top half than from the bottom half of the gradient. In conjunction with this, the distribution of both raft markers and nonraft markers is altered. Flotillin (Fig. 2B) appears to be excluded in c6 cells (fraction 2) or reduced in neuroblastomas (fractions 3 and 4) from certain DRM fractions relative to other fractions. CtxB's affinity for isolated DRM fractions (Fig. 2C) also appears to be affected by cholesterol depletion; in the neuroblastomas, CtxB shows diminished interaction with DRM fractions 1 and 2 upon M $\beta$ CD treatment. Likewise in c6 cells, M $\beta$ CD treatment causes CtxB's interaction with DRMs (fractions 1 and 2) to be weakened. In addition to the decreased association with DRM fractions 1 and 2 in c6 cells, the raft markers flotillin and CtxB both appear to concentrate in fraction 4 upon cholesterol depletion. Conversely, the nonraft marker rac (Fig. 2B), which is normally excluded from DRM fractions, appears to now distribute in these fractions (2, 3), suggesting that cholesterol depletion has indeed affected the partitioning of both raft and nonraft proteins in the membrane of c6 cells.

SBD uptake into DRMs is also affected by M $\beta$ CD treatment. Cholesterol depletion by M $\beta$ CD caused a reduced uptake of SBD in some of the DRM fractions of c6 cells (fractions 2 and 4) and of neuroblastomas (fraction 4) (Fig. 2D). Together, these results suggest that the DRM association for SBD is more dependent on cholesterol in some cell types than in others and that some SBD also associates with fractions that do not fulfill the criteria for DRM fractions. SBD's only partial cholesterol dependence for raft association is not unique; another raft marker, flotillin, is also reported to be resistant to cholesterol depletion (28).

The effect of cholesterol depletion on SBD uptake within 30 min is less dramatic on neuroblastomas than in c6 cells (Fig. 2D). In light of our observations that SBD is continuously taken up by neuroblastomas, we wondered whether SBD uptake over prolonged time periods is more susceptible to cholesterol depletion in these cells. Our results (see supplementary Fig. I) indicate that there is no obvious difference in the cholesterol dependence of SBD uptake at 30 or 60 min.

The above data support the conclusion that SBD's membrane association is in general influenced by cholesterol, but depletion of cholesterol does not inhibit its association with DRM-isolatable microdomains equally in all

cells. However, the trend of flattening of the cholesterol levels and change in SBD distributions across fractions, upon cholesterol depletion, was observed consistently (see supplementary Fig. II).

### Cholesterol depletion inhibits SBD uptake

Having determined that cholesterol depletion altered the association of SBD with DRMs, we wanted to find out whether the distribution and uptake of SBD in live cells was detectably altered by cholesterol inhibition. To do this, we imaged SBD-TMR (SBD-TMR) uptake by c6 and SH-SY5Y neurons upon M $\beta$ CD treatment. Normally, c6 cells internalize SBD within minutes (S. Steinert and E. Lee, unpublished data) (Fig. 3), leaving little signal at the plasma membrane. In contrast, SBD uptake in M $\beta$ CD-treated c6 cells was strongly inhibited (Fig. 3A–C), as indicated by a substantial reduction in the number of internalized SBD-positive spots after cholesterol depletion and more fluorescence at the plasma membrane. Cholesterol depletion was monitored by the assays shown in Fig. 2 and by filipin staining of treated, fixed cells (Fig. 3B, C). SBD uptake at the plasma membrane of cholesterol-depleted SH-SY5Y neuroblastomas was also strongly disrupted; this is reflected in the lag in uptake (Fig. 3D) and in the strongly reduced number of cells containing SBD-positive vesicles after 1 h (Fig. 3D–F). In the same cells, CtxB-Alexa-594 (Invitrogen) also showed a reduced rate of uptake, with a smaller number of internal vesicles, but only after 2 h of cholesterol depletion (data not shown). These results demonstrate that efficient SBD vesicular uptake requires cholesterol (or other sterols) in both *Drosophila* and mammalian neurons.

### FCS analysis of SBD shows plasma membrane mobility characteristic of raft markers

To compare the mobility of SBD on the plasma membrane with that of other raft- and nonraft-associated markers, we carried out FCS measurements on the diffusion rate of SBD-TMR at the plasma membrane of SH-SY5Y neuroblastoma cells. FCS records fluorescence autocorrelation functions,  $G(\tau)$ , from a diffraction-limited confocal volume centered on the upper plasma membrane of the cell. Depending on the number of different fluorescent particle species passing through the confocal volume and their location with respect to the plasma membrane, different models may be used to fit  $G(\tau)$ , incorporating one or more particles with different mobilities in two or three dimensions (i.e., one particle vs. two particles and two dimensions vs. three dimensions). The diffusion time,  $\tau_D$ , is derived from the autocorrelation curve  $G(\tau)$  and gives the time taken by the fluorescent probe to cross the stationary confocal volume. A multiple particle fit will result in a number of diffusion times, which are inversely proportional to the diffusion coefficients. The  $\tau_D$  is characteristic of the viscosity in which the membrane probe resides and thus can be used to predict the membrane domain localization of the probe (29).

Measurements were taken for SBD-TMR, SBD-OG, the raft marker CtxB-Alexa-594, and the nonraft mark-



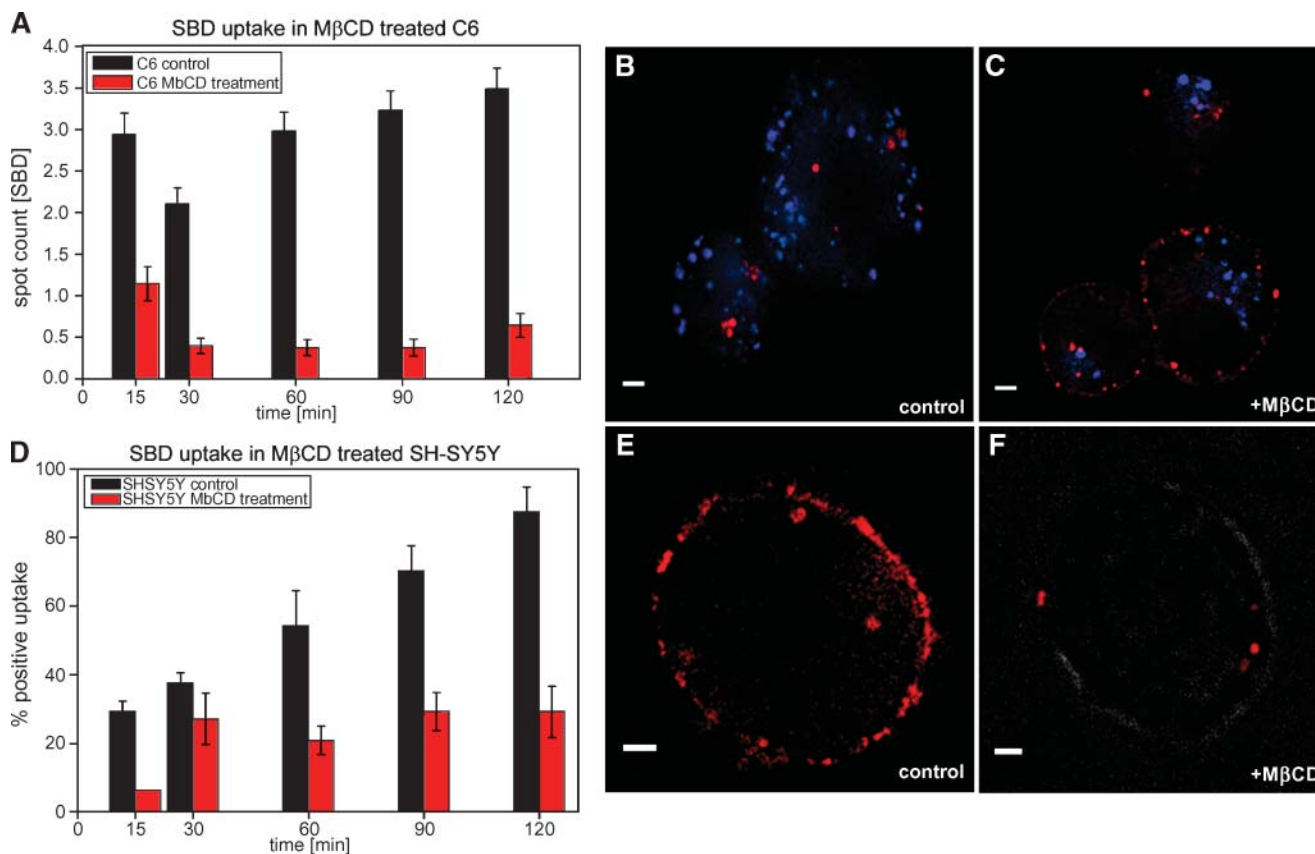


**Fig. 3.** SBD uptake at the plasma membrane is cholesterol-dependent. **A:** Average number of SBD-tetramethyl rhodamine (TMR)-positive vesicles per cell in live c6 neurons untreated (black bars) or treated (red bars) with 10 mM M $\beta$ CD. Cholesterol depletion significantly decreases the uptake of SBD over the indicated time course (see Fig. 2 for the quantitation of cholesterol levels). **B, C:** Fixed c6 neurons showing filipin staining of cholesterol (blue) and SBD (red) after 30 min of SBD incubation. In cholesterol-depleted neurons (**C**), SBD remains predominantly at the plasma membrane. **D:** Average percentages of live cells with internalized SBD in SH-SY5Y cells untreated (black bars) or treated with 10 mM M $\beta$ CD (red bars). In contrast to the gradual increase of SBD uptake in controls, cholesterol depletion prevents SBD uptake. **E, F:** Live SH-SY5Y cells showing reduced incorporation and uptake at the plasma membrane of SBD, as measured by the presence or absence of internalized SBD-positive vesicles within the cell, at 60 min after incubation with 10  $\mu$ M M $\beta$ CD. Bars = 2  $\mu$ m. Error bars represent  $\pm$  SEM.

ers DiI-C18 and BODIPY-FL-SM (30, 31) (**Fig. 4**). The  $G(\tau)$  functions obtained for these measurements were fitted with a model taking into account the two-dimensional diffusion of two distinct particles and possibly a third particle representing free three-dimensional diffusion of unbound labels. The two two-dimensional diffusing species are interpreted as a faster moving, nonraft-associated population of SBD label in the plasma membrane in addition to a less mobile, raft-associated component. As a control for contributions to  $G(\tau)$  from free label in the medium (outside the cell) or autofluorescence (inside the cell), additional measurements were made outside and inside the cell, with resulting diffusion times of  $94 \pm 2 \mu$ s and  $2.2 \pm 0.2$  ms, respectively. Values outside the cell are fitted to a three-dimensional, one-particle model, and values inside the cell are fitted to a three-dimensional, two-particle model, as a result of contributions from autofluorescence. Because the correlation time for membrane-associated markers is not expected to be smaller than the millisecond range (the  $\tau_D$  for DiI, a typical nonraft membrane probe, was  $10 \pm 0.4$  ms) and that for the free label in solution is observed to be in the  $\sim 100 \mu$ s

range, those readings that are dominated by this component were removed from the calculation of average  $\tau_D$ .

In agreement with the findings of Schwille and colleagues (29), measurements of the raft marker CtxB-Alexa594 were influenced by bleaching effects, presumably as a result of the low mobility of the protein in raft domains (**Fig. 4**). The distributions of  $\tau_D$  of SBD-TMR and SBD-OG were found to be mainly in the  $>30$  ms category (SBD-TMR,  $\sim 70$  ms; SBD-OG,  $\sim 60$  ms on average), with a slightly greater contribution from slow-moving particles than CtxB ( $\sim 25$  ms) (**Fig. 5B**). We found that SBD-TMR and SBD-OG measurements, similar to CtxB, were strongly influenced by bleaching. To separate these effects, which artificially bias the  $\tau_D$  toward faster moving particles, we expressed the  $\tau_D$  frequencies as histograms. In contrast to the longer  $\tau_D$  (slower diffusion) of the raft markers, the  $\tau_D$  of DiI-C18, a nonspecific lipophilic dye, and BODIPY-FL-SM, a nonraft-localizing sphingolipid analog (32), were distributed to a large extent between 1 and 20 ms (**Fig. 5A**), with the main contribution being 1–10 ms ( $10 \pm 0.4$  ms for DiI-C18,  $10 \pm 2$  ms for BODIPY-FL-SM on average; **Fig. 5E**). The histograms also reveal a biphasic

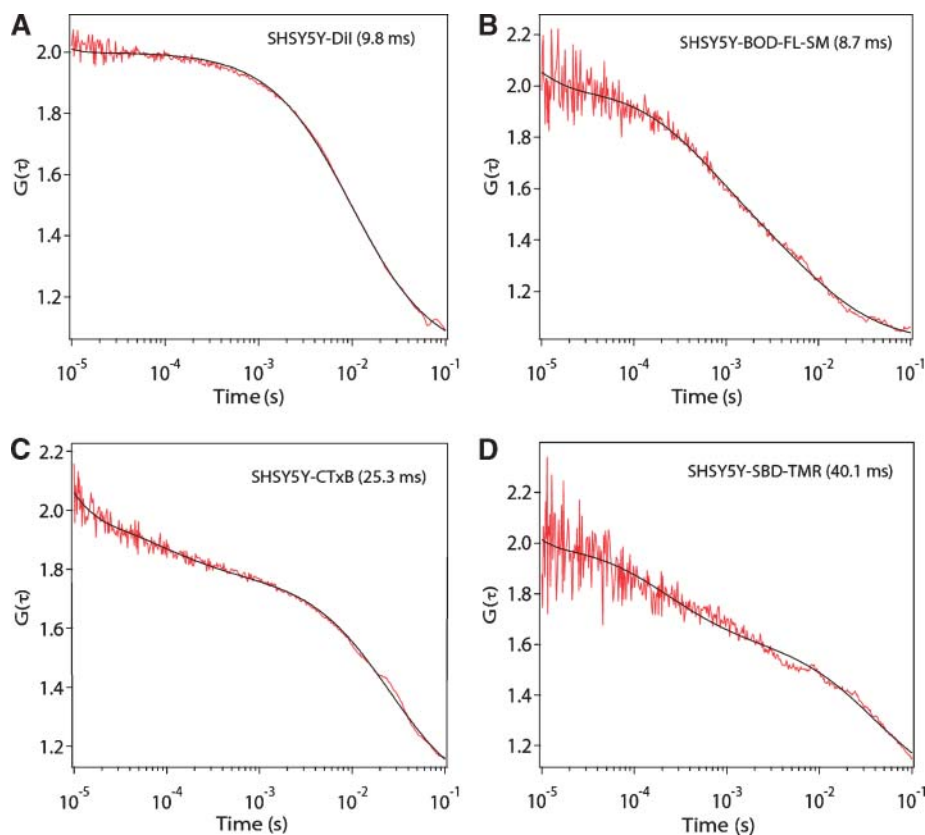


**Fig. 4.** Correlation curves of SBD (SBD-TMR; D) versus raft (CtxB; C) and nonraft markers (DiI-C18; A; and BODIPY-FL-SM; B) in SH-SY5Y cells. Normalized correlation curves  $G(\tau)$  are shown over 100 ms time intervals obtained from different fluorescent labels on SH-SY5Y neuroblastoma cells. Functions gave the best fits to two-dimensional, two-particle models. SBD and CtxB contain a strong bleaching component, indicating the lower mobility of the structures in which they reside, whereas dialkyl-indocarbocyanine (DiI)-C18 and BODIPY-FL-SM were not influenced by bleaching.

distribution that is strikingly similar for CtxB and SBD-OG, with a slow population diffusing at  $>30$  ms and a slightly larger fast population diffusing mainly between 1 and 10 ms. This is less pronounced for SBD-TMR.

To look at the effects of raft disruption on the mobility of SBD, we measured the  $\tau_D$  of SBD as well as the control markers on cells treated with 10 mM M $\beta$ CD for 30 min. It was found that the diffusion times of DiI and BODIPY-FL-SM under cholesterol depletion remained almost unchanged at  $10.7 \pm 0.6$  and  $11.5 \pm 2.9$  ms, respectively (Fig. 5E, F), whereas  $\tau_D$ s of SBD were greatly reduced to  $5.3 \pm 0.9$  and  $2.1 \pm 0.2$  ms for SBD-TMR and SBD-OG, respectively (Fig. 5F). The average diffusion time of CtxB was also reduced to  $11.6 \pm 0.8$  ms, consistent with its raft localization being dependent on cholesterol (Fig. 5F). These changes are also reflected in the distributions of  $\tau_D$ s represented as histograms (Fig. 5C, D). From the FCS data, we conclude that SBD's diffusion behavior at the plasma membrane is consistent with a substantial fraction being localized in raft domains of low mobility relative to the surrounding membrane.

#### Sphingolipid depletion inhibits SBD uptake

The SBD motif was postulated to interact with galactose-terminal glycosphingolipids and sphingomyelin (33), and

A $\beta$  interactions with gangliosides have been documented extensively (34, 35). Therefore, we examined with live cell imaging whether the vesicular uptake of SBD requires sphingolipid production in neuroblastomas. Sphingolipid metabolism is disrupted by the mycotoxin FB1, an inhibitor of ceramide synthase (36), a key enzyme in de novo ceramide synthesis. Because glycosphingolipids are synthesized from ceramide, a reduction in ceramide levels should also lead to decreased levels of glycosphingolipids, and inhibition of cellular ganglioside synthesis has indeed been reported upon treatment with FB1 (37, 38). After treatment with FB1, neuroblastoma cells endocytosed SBD less efficiently and showed fewer internal SBD-positive vesicles (Fig. 6D; quantitated in Fig. 6C) as well as a decrease in total intracellular SBD intensity (quantification shown in supplementary Fig. III), suggesting that the vesicular uptake of SBD is dependent on sphingolipids or glycosphingolipids.

By comparison, the distribution of the positive control CtxB, which recognizes ganglioside GM1 (39), is also altered, but apparently uptake is not affected. Instead, CtxB appears to be diverted from its usual Golgi localization (Fig. 6E). Both of these observations are consistent with the conclusions of Shogomori and Futerman (7), who found that CtxB is raft-localized but that uptake can be



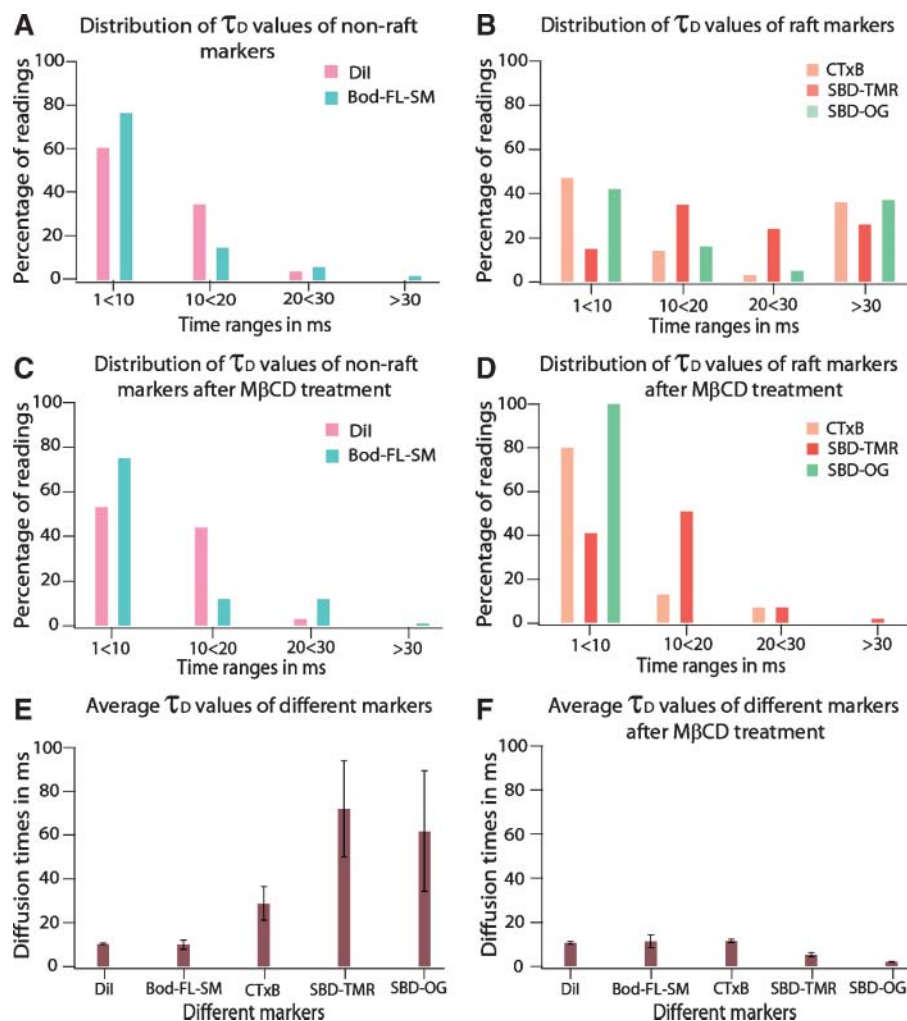


**Fig. 5.** The distribution of diffusion times for SBD and raft markers but not nonraft markers shifts under cholesterol depletion. Histograms A–D show percentages of 20 s cumulative average readings that gave  $\tau_D$  in the indicated millisecond time ranges. A shows the nonraft-localizing markers DiI and BODIPY-FL-SM, which give most of the readings in the faster mobility ranges 1–10 and 10–20 ms. In contrast, in B, CtxB-594, SBD-TMR, and SBD-Oregon green (OG) give substantial fractions of readings in the low-mobility >30 ms range, typical for raft markers, in addition to a higher proportion of readings for SBD in the faster 1–20 ms range. Note that all readings >30 ms are pooled into one group in the histograms, because of possible artifactual lengthening of the  $\tau_D$  at >30 ms as a result of photobleaching effects. C: Distribution of nonraft markers after cholesterol depletion is not altered significantly (compare with A). D: Distribution of raft markers after cholesterol depletion is shifted strongly toward faster diffusion times (<1–10 ms). E, F: Average diffusion times for all markers before and after cholesterol depletion. Error bars reflect SEM. For all experiments,  $n > 50$  measurements.

raft-independent. In contrast, transferrin-Alexa-594 uptake (Fig. 6A, B) remains unaltered after FB1 treatment. Transferrin was measured on the same cells as a negative control for the FB1 treatment, because transferrin is taken up by clathrin-mediated endocytosis and therefore is not expected to be sphingolipid-dependent (40, 41).

We also examined SBD uptake in a melanoma strain, GM95 (42), which is devoid of glycosphingolipids. However, uptake of SBD was extremely inefficient in both the parental/control melanoma cell line, B16, and the mutant GM95 strain (data not shown), such that no conclusions could be drawn about the dependence of SBD uptake on glycosphingolipids in this cell type.

### SBD binds to purified glycosphingolipids

Previous *in vitro* binding studies on SBDs contained in HIV-GP120 and Prp (prion-protein), and A $\beta$ (1–40) (13, 33) suggested that the association of these proteins with cell membranes could be mediated by interactions between the SBD and glycosphingolipids at the outer plasma membrane, in particular those containing terminal galactose. For this reason, we were interested in testing whether our myc-tagged SBD could bind to isolated glycosphingolipids. Interaction of SBD with lipids was assayed by lipid-protein overlays (16) in which SBD-myc was incubated with purified lipids immobilized on nitrocellulose membranes. With relatively low amounts of lipid (100 pmoles), SBD

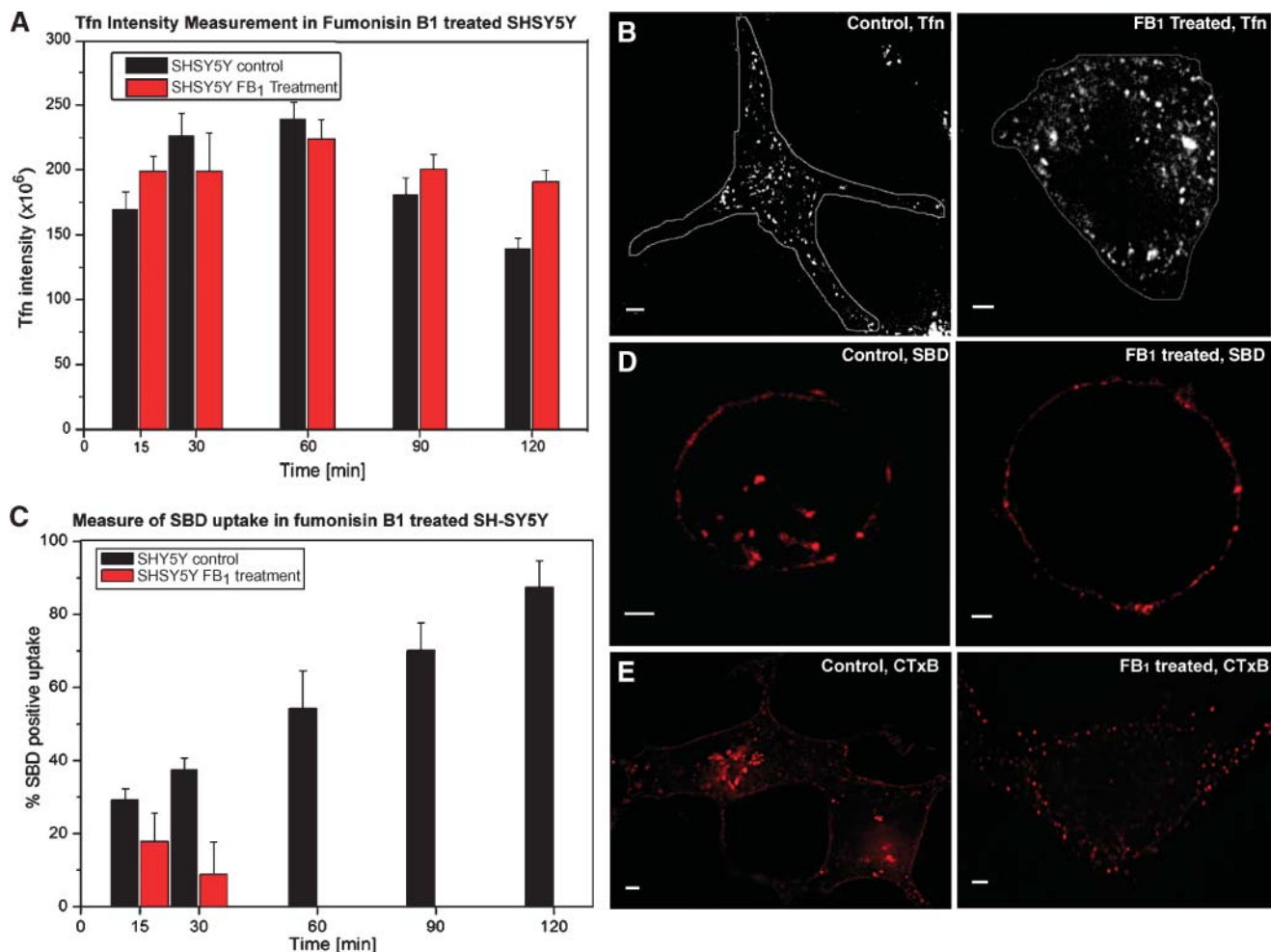


**Fig. 6.** SBD uptake is dependent on sphingolipid levels. SH-SY5Y cells were treated with 10  $\mu$ M fumonisin B1 (FB1) for 2 h and then incubated with transferrin-Alexa-594 (Tfn), SBD-TMR, or Alexa Fluor-594 CtxB and subsequently imaged in medium containing 10  $\mu$ M FB1. **A:** FB1 treatment does not significantly alter the uptake of Tfn. The graph shows the intensity measurement after Tfn uptake at specific time points in treated (red bars) and untreated (black bars) cells. **B:** Representative cells used for the analysis of Tfn uptake, with the cell boundary outlined. The intensity of spots within the cell was measured and compared between treated and control cells. **C:** SBD uptake is reduced as indicated by spot count analysis. The graph indicates the percentage of SBD-positive spots in FB1-treated (red bars) and control cells (black bars). Spot count was used as a direct measurement of uptake instead of intensity because of the relatively lower uptake of SBD into SH-SY5Y cells compared with that of SBD into c6 cells (see supplementary Fig. II). **D:** Representative SH-SY5Y cells before and after FB1 treatment incubated with SBD-TMR. Fewer internal vesicles, carrying internalized SBD, are seen in the treated cells, where SBD remains at the plasma membrane. **E:** Control and FB1-treated cells show differences in CtxB trafficking. CtxB is ordinarily trafficked to the Golgi body, seen near the center of neuroblastoma cells, but in FB1-treated cells, this is altered to a vesicular distribution throughout the cell. Bars = 2  $\mu$ m.

recognized GM1 but not a variety of other glycosphingolipids, glycerophospholipids, or cholesterol (Fig. 7A). Intact SBD and SBD with a scrambled sequence showed signal for GM1, but much lower than the signal of Lysenin for sphingomyelin (Fig. 7A) or of CtxB on its receptor GM1 (data not shown). However when higher amounts of lipids were used (between 1,000 and 2,000 pmoles), SBD displayed an interaction with galactocerebrosides and gangliosides GD1a and GD1b and, to a much lesser extent, with sphingomyelin (Fig. 7B). No other lipids or sphingolipids displayed an interaction with SBD, including cholesterol, sulfatide, disialoganglioside, and trisialoganglioside (GM3) (Fig. 7A, B). Notably, although SBD interacted strongly with bovine galactocerebrosides (consisting of a mixture of both hydroxylated and nonhydroxylated fatty

acids) (Fig. 7B), it showed no affinity for synthetic galactosyl ceramide, which has an essentially identical structure but contains only nonhydroxylated fatty acids. This is not completely unexpected, because another SBD-containing glycoprotein, the HIV-1 surface protein gp120, also displays preferential interaction with synthetic galactosyl ceramide containing hydroxylated fatty acid (43).

We also examined the interaction of the scrambled version of the peptide and a double mutant version in which amino acids key to the interaction with sphingolipids postulated by Fantini and colleagues (33) were mutated (Fig. 7B). Surprisingly, the scrambled version of the peptide interacted approximately as well with GD1a, GD1b, and SM as native SBD. This is consistent with the reported binding affinity for target lipids of reverse-sequence A $\beta$ 40-1

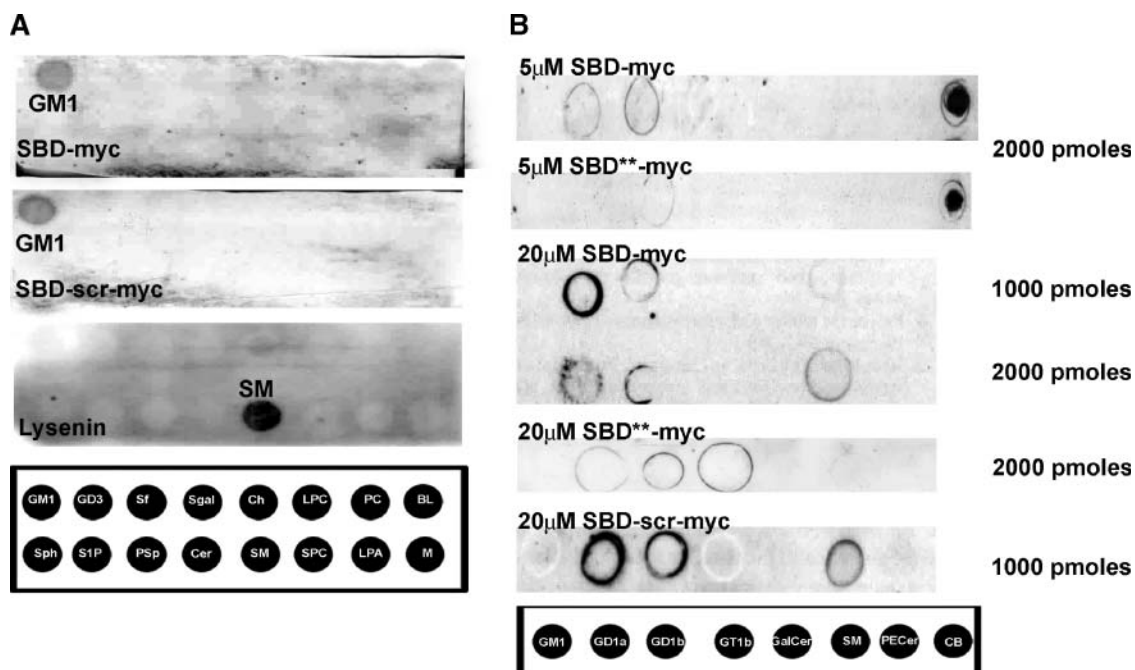


**Fig. 7.** SBD interacts with purified glycosphingolipids. **A:** Lipid-protein overlay assay using Sphingostrips (Invitrogen) prespotted with lipids and exposed to SBD-myc, SBD with a scrambled sequence (SBD-scr)-myc, and Lysenin. SBD-myc and SBD-scr-myc interact with monosialoganglioside (GM1). Lysenin recognizes its known target, sphingomyelin (SM). GD3, disialoganglioside; Sf, sulfatide; Sgal, sphingosylgalactoside; Ch, cholesterol; LPC, lysophosphatidylcholine; PC, phosphatidylcholine; BL, blank; Sph, sphingosine; S1P, sphingosine-1-phosphate; PSp, phytosphingosine; Cer, ceramide; SPC, sphingosylphosphocholine; LPA, lysophosphatidic acid; M, myriocin. **B:** Lipid-protein overlay assay using membrane strips spotted with additional sphingolipid standards and then exposed to SBD-myc (5 and 20  $\mu$ M), SBD mutated (SBD\*\*)-myc, and SBD-scr-myc. SBD-myc and SBD-scr-myc bind to GD1a, GD1b, and galactocerebrosides. SBD-myc weakly interacts with SM at higher concentrations (20  $\mu$ M). Double mutated (R5A, Y10A) SBD\*\*)-myc fails to show any interaction with GD1a and SM at 5  $\mu$ M. At higher concentrations (20  $\mu$ M), it fails to show any interaction with SM and only weakly interacts with GD1a, GD1b, and GT1b. GD1a, disialoganglioside 1a; GD1b, disialoganglioside 1b; GT1b, trisialoganglioside GT1b; GalCer, galactosyl ceramide; PE-Cer, phosphoethanolamine ceramide; CB, galactosylcerebroside.

being comparable to, or even exceeding that of, A $\beta$ 1-40 in SPR measurements (34). However, in contrast to live cell labeling with native SBD, nearly no uptake was observed with the scrambled SBD peptide (see supplementary Fig. IV). Our interpretation of these seemingly contradictory results is that SBD may bind weakly to individual gangliosides but more strongly to a specific combination of gangliosides or lipids that we have not yet been able to reproduce on dot blots. SBD may also interact with an unknown protein in the membrane to confer sequence-specific binding.

In contrast, the double mutated version (R5A, Y10A) interacted only with GD1b very weakly and with galactocerebrosides. At higher concentrations, the mutated peptide bound very weakly to GD1a but not to SM. We conclude from this that the interaction between SBD and gangliosides or SM may indeed be mediated at least in part by these two amino acids, as postulated by Fantini and colleagues (33).

## DISCUSSION

We have presented biochemical and pharmacological evidence that a novel fluorescent probe derived from the amyloid peptide A $\beta$ , the SBD, associates with plasma membrane microdomains. SBD is taken up by two different

neuronal cell types in a cholesterol- and sphingolipid-dependent manner.

We show that SBD is associated with microdomains of both fly neuronal cells and mammalian neuroblastomas, but not fibroblasts, and we also observe that its association with DRMs is partly cholesterol dependent in both cell types, with fly neurons being more sensitive to cholesterol depletion. In light of this, it is interesting that sphingolipids in flies are structurally different from their mammalian counterparts (24). Although flies do not produce sphingomyelin or gangliosides such as GM1, they have other terminal galactose-containing glycolipids (44) and an analog of sphingomyelin, phosphoethanolamine ceramide, that could also be cleaved by sphingomyelinases (22; Julie Saba, personal communication). These fly sphingolipids could be involved in cholesterol dependent SBD uptake.

We also analyzed the biophysical characteristics of SBD's association with the plasma membrane by examining its diffusion dynamics with FCS in human neuroblastomas. In this study, the  $\tau_D$ s of the nonraft markers (DiI and BODIPY-FL-SM) were distributed within a comparatively narrow range, unlike the raft markers, which were distributed in a very wide range of  $\tau_D$  values. However, the clustering of the histogram of SBD  $\tau_D$  values around >30 ms and ~1–10 ms is consistent with the estimates of




Sharma et al. (45) that 60–80% of a raft-associated glycosylphosphatidylinositol-linked protein is actually present in the nonraft fraction. The very similar biphasic distribution of diffusion times for SBD (in particular SBD-OG) and CtxB may reflect the existence of two distinct populations at the plasma membrane, one of which is associated with the liquid-ordered phase and the other not. Indeed, from our fractionation experiments, we observe that SBD is also taken up by membrane components that do not fit within the operative definition for rafts, namely, detergent insolubility. This mixed distribution is observed by us and other authors for a number of presumed raft-associated proteins (46).

It is interesting that although the clustered histogram distribution of  $\tau_D$  values of CtxB was very similar to those of SBD, especially SBD-OG, the average  $\tau_D$  for this established raft marker was shorter on average than those of SBD (Fig. 5B). This may indicate that CtxB and SBD are both at least partially raft-associated but that the dynamic nature of their resident domains is different. Raft-associated markers are expected to be bleached, because they are less mobile than the surrounding nonraft membrane and thus are unable to leave the focus (47, 48). Accordingly, we see a major bleaching component in our measurements of SBD and CtxB. The extremely slow mobile fraction observed for SBD and CtxB compared with DiI, therefore, suggests their association to raft-like structures or cross-linked raft assemblies.

Drugs that remove cholesterol from the plasma membrane are known to inhibit the trafficking of lipid raft markers and have been used extensively as tools to differentiate between raft- and nonraft-mediated processes (47, 49). Both biochemical and cell-labeling studies indicate a cholesterol-dependent uptake of SBD. However, this difference is more obvious in the c6 cells than in the neuroblastomas. Using FCS on neuroblastomas, under cholesterol depletion, the influence of bleaching on the autocorrelation function is in fact removed, and we find a large change in  $\tau_D$  value for SBD. The shift is toward nonraft-like fast diffusion times. This is similar to the effect on the raft marker CtxB, whereas the nonraft markers did not show any significant change (29). Taking into consideration both the DRM isolation data and the FCS results, we conclude that SBD is still able to associate to some extent with the more buoyant membrane fractions, even in the absence of cholesterol and diffusing at nonraft speeds.

In a separate study, we showed that SBD interacts with ganglioside-containing liposomes of raft-like composition (S. Steinert and E. Lee, unpublished data). Here, we used a more sensitive (50) lipid-protein overlay (fat blot) assay to assess SBD's ability to bind specific lipids. Among the sphingolipids we tested by lipid-protein overlay, SBD bound to galactocerebrosides and to GD1a, GD1b, and GM1 but not to other sphingolipids. SBD's affinity for glycosphingolipids, but not cholesterol, glycerophospholipids, or sphingoid bases, is consistent with the original model of Fantini and coworkers (33) that SBD binds to rafts primarily via an interaction with raft-borne glycosphingolipid head groups.

SBD also displayed a weak interaction with sphingomyelin. Interestingly, a double mutation (in which arginine 5 and tyrosine 10 are both switched to alanine) eliminated the interaction with sphingomyelin. This supports the prediction (13) that secondary electrostatic interactions involving basic charged residues such as lysine and arginine with the negatively charged phosphate group of sphingomyelin are also possible. The same double mutant also affected SBD's ability to bind gangliosides, again supporting the model of Fantini and coworkers (33), in which aromatic amino acids in the V3 loop engage in  $\pi$ -bonding with galactose found in galactose-containing head groups. In addition, all three peptides interact with brain-derived galactocerebrosides but not galactosyl ceramide. In light of our liposome-capture experiments (S. Steinert and E. Lee, unpublished data), however, in which SBD did not bind galactocerebrosides, it seems likely that this interaction is not physiological and may occur only when the lipids are not presented in a bilayer.

In a separate study (S. Steinert and E. Lee, unpublished data) using quantitative time-lapse imaging, we characterized the intracellular trafficking pathway of SBD and showed that it could interact with a number of different cell types and certain glycolipids in liposome-capture experiments. The current studies used three approaches to describe SBD's behavior at the plasma membrane. First, we used lipid-protein interaction assays with DRM fractions and fat blots to determine SBD's affinity for raft-type lipids. Second, pharmacological inhibitor studies were used to test the cholesterol and glycosphingolipid dependence of SBD uptake at the membrane. Finally, we used FCS to show that SBD displays a low mobility at the membrane, characteristic of raft-associated markers. These studies, along with the intracellular trafficking characterization, establish SBD as a novel fluorescent tracer for cholesterol-dependent, glycosphingolipid-containing microdomains in living cells. 

The authors thank Sean Sweeney and Laura Briggs for flotillin-GFP plasmid. Funding for this project was provided by the Institute of Bioengineering and Nanotechnology (Biomedical Research Council, Agency for Science, Technology, and Research, Singapore) and the Singapore Bioimaging Consortium (Grant 003/2005). M.M. was supported by a National University of Singapore graduate scholarship.

## REFERENCES

1. Simons, K., and E. Ikonen. 1997. Functional rafts in cell membranes. *Nature*. **387**: 569–572.
2. Brown, D. A., and E. London. 1998. Functions of lipid rafts in biological membranes. *Annu. Rev. Cell Dev. Biol.* **14**: 111–136.
3. Simons, K., and R. Ehehalt. 2002. Cholesterol, lipid rafts, and disease. *J. Clin. Invest.* **110**: 597–603.
4. Glebov, O. O., N. A. Bright, and B. J. Nichols. 2006. Flotillin-1 defines a clathrin-independent endocytic pathway in mammalian cells. *Nat. Cell Biol.* **8**: 46–54.
5. Lencer, W. I., and D. Saslowsky. 2005. Raft trafficking of AB5 subunit bacterial toxins. *Biochim. Biophys. Acta.* **1746**: 314–321.
6. Sabharanjak, S., P. Sharma, R. G. Parton, and S. Mayor. 2002. GPI-anchored proteins are delivered to recycling endosomes via a

- distinct cdc42-regulated, clathrin-independent pinocytic pathway. *Dev. Cell.* **2**: 411–423.
7. Shogomori, H., and A. H. Futerman. 2001. Cholesterol depletion by methyl-beta-cyclodextrin blocks cholera toxin transport from endosomes to the Golgi apparatus in hippocampal neurons. *J. Neurochem.* **78**: 991–999.
  8. Torgersen, M. L., G. Skretting, B. van Deurs, and K. Sandvig. 2001. Internalization of cholera toxin by different endocytic mechanisms. *J. Cell Sci.* **114**: 3737–3747.
  9. Drobnik, W., H. Borsukova, A. Bottcher, A. Pfeiffer, G. Liebisch, G. J. Schutz, H. Schindler, and G. Schmitz. 2002. Apo AI/ABCA1-dependent and HDL3-mediated lipid efflux from compositionally distinct cholesterol-based microdomains. *Traffic.* **3**: 268–278.
  10. Gomez-Mouton, C., J. L. Abad, E. Mira, R. A. Lacalle, E. Gallardo, S. Jimenez-Baranda, I. Illa, A. Bernad, S. Manes, and A. C. Martinez. 2001. Segregation of leading-edge and uropod components into specific lipid rafts during T cell polarization. *Proc. Natl. Acad. Sci. USA.* **98**: 9642–9647.
  11. Ishitsuka, R., and T. Kobayashi. 2004. Lysenin: a new tool for investigating membrane lipid organization. *Anat. Sci. Int.* **79**: 184–190.
  12. Schade, A. E., and A. D. Levine. 2002. Lipid raft heterogeneity in human peripheral blood T lymphoblasts: a mechanism for regulating the initiation of TCR signal transduction. *J. Immunol.* **168**: 2233–2239.
  13. Fantini, J. 2003. How sphingolipids bind and shape proteins: molecular basis of lipid-protein interactions in lipid shells, rafts and related biomembrane domains. *Cell. Mol. Life Sci.* **60**: 1027–1032.
  14. Ui, K., S. Nishihara, M. Sakuma, S. Togashi, R. Ueda, Y. Miyata, and T. Miyake. 1994. Newly established cell lines from *Drosophila* larval CNS express neural specific characteristics. *In Vitro Cell. Dev. Biol. Anim.* **30A**: 209–216.
  15. Zhai, L., D. Chaturvedi, and S. Cumberledge. 2004. *Drosophila* wnt-1 undergoes a hydrophobic modification and is targeted to lipid rafts, a process that requires porcupine. *J. Biol. Chem.* **279**: 33220–33227.
  16. Dowler, S., G. Kular, and D. R. Alessi. 2002. Protein lipid overlay assay. *Sci. STKE.* **2002**: PL6.
  17. Sharma, D. K., J. C. Brown, Z. Cheng, E. L. Holicky, D. L. Marks, and R. Pagano. 2005. The glycosphingolipid, lactosylceramide, regulates B1-integrin clustering and endocytosis. *Cancer Res.* **65**: 8233–8241.
  18. Bacia, K., and P. Schwille. 2003. A dynamic view of cellular processes by in vivo fluorescence auto- and cross-correlation spectroscopy. *Methods.* **29**: 74–85.
  19. Haustein, E., and P. Schwille. 2003. Ultrasensitive investigations of biological systems by fluorescence correlation spectroscopy. *Methods.* **29**: 153–166.
  20. Edidin, M. 2003. The state of lipid rafts: from model membranes to cells. *Annu. Rev. Biophys. Biomol. Struct.* **32**: 257–283.
  21. Hoehne, M., H. G. de Couet, C. A. Stuermer, and K. F. Fischbach. 2005. Loss- and gain-of-function analysis of the lipid raft proteins Reggie/Flotillin in *Drosophila*: they are posttranslationally regulated, and misexpression interferes with wing and eye development. *Mol. Cell. Neurosci.* **30**: 326–338.
  22. Rietveld, A., S. Neutz, K. Simons, and S. Eaton. 1999. Association of sterol- and glycosylphosphatidylinositol-linked proteins with *Drosophila* raft lipid microdomains. *J. Biol. Chem.* **274**: 12049–12054.
  23. Li, Y. P., A. F. Bushnell, C. M. Lee, L. S. Perlmutter, and S. K. Wong. 1996. Beta-amyloid induces apoptosis in human-derived neurotypic SH-SY5Y cells. *Brain Res.* **738**: 196–204.
  24. Holthuis, J. C., T. Pomorski, R. J. Riggers, H. Sprong, and G. Van Meer. 2001. The organizing potential of sphingolipids in intracellular membrane transport. *Physiol. Rev.* **81**: 1689–1723.
  25. Yamaji, A., Y. Sekizawa, K. Emoto, H. Sakuraba, K. Inoue, H. Kobayashi, and M. Umeda. 1998. Lysenin, a novel sphingomyelin-specific binding protein. *J. Biol. Chem.* **273**: 5300–5306.
  26. Ohanian, J., and V. Ohanian. 2001. Sphingolipids in mammalian cell signalling. *Cell. Mol. Life Sci.* **58**: 2053–2068.
  27. Puri, V., R. Watanabe, R. D. Singh, M. Dominguez, J. C. Brown, C. L. Wheatley, D. L. Marks, and R. E. Pagano. 2001. Clathrin-dependent and -independent internalization of plasma membrane sphingolipids initiates two Golgi targeting pathways. *J. Cell Biol.* **154**: 535–547.
  28. Rajendran, L., M. Masilamani, S. Solomon, R. Tikkanen, C. A. Stuermer, H. Plattner, and H. Illges. 2003. Asymmetric localization of flotillins/reggies in preassembled platforms confers inherent polarity to hematopoietic cells. *Proc. Natl. Acad. Sci. USA.* **100**: 8241–8246.
  29. Bacia, K., D. Scherfeld, N. Kahya, and P. Schwille. 2004. Fluorescence correlation spectroscopy relates rafts in model and native membranes. *Biophys. J.* **87**: 1034–1043.
  30. Kahya, N., D. Scherfeld, K. Bacia, B. Poolman, and P. Schwille. 2003. Probing lipid mobility of raft-exhibiting model membranes by fluorescence correlation spectroscopy. *J. Biol. Chem.* **278**: 28109–28115.
  31. Burns, A. R., D. J. Frankel, and T. Buranda. 2005. Local mobility in lipid domains of supported bilayers characterized by atomic force microscopy and fluorescence correlation spectroscopy. *Biophys. J.* **89**: 1081–1093.
  32. Hao, M., S. Mukherjee, and F. R. Maxfield. 2001. Cholesterol depletion induces large scale domain segregation in living cell membranes. *Proc. Natl. Acad. Sci. USA.* **98**: 13072–13077.
  33. Mahfoud, R., N. Garmy, M. Maresca, N. Yahi, A. Puigserver, and J. Fantini. 2002. Identification of a common sphingolipid-binding domain in Alzheimer, prion, and HIV-1 proteins. *J. Biol. Chem.* **277**: 11292–11296.
  34. Ariga, T., K. Kobayashi, A. Hasegawa, M. Kiso, H. Ishida, and T. Miyatake. 2001. Characterization of high-affinity binding between gangliosides and amyloid beta-protein. *Arch. Biochem. Biophys.* **388**: 225–230.
  35. Kakio, A., S. Nishimoto, K. Yanagisawa, Y. Kozutsumi, and K. Matsuzaki. 2002. Interactions of amyloid beta-protein with various gangliosides in raft-like membranes: importance of GM1 ganglioside-bound form as an endogenous seed for Alzheimer amyloid. *Biochemistry.* **41**: 7385–7390.
  36. Merrill, A. H., Jr., G. van Echten, E. Wang, and K. Sandhoff. 1993. Fumonisin B1 inhibits sphingosine (sphinganine) N-acyltransferase and de novo sphingolipid biosynthesis in cultured neurons in situ. *J. Biol. Chem.* **268**: 27299–27306.
  37. Merrill, A. H., Jr., E. Wang, T. R. Vales, E. R. Smith, J. J. Schroeder, D. S. Menaldino, C. Alexander, H. M. Crane, J. Xia, D. C. Liotta, et al. 1996. Fumonisin toxicity and sphingolipid biosynthesis. *Adv. Exp. Med. Biol.* **392**: 297–306.
  38. Naslavsky, N., H. Shmeeda, G. Friedlander, A. Yanai, A. H. Futerman, Y. Barenholz, and A. Taraboulos. 1999. Sphingolipid depletion increases formation of the scrapie prion protein in neuroblastoma cells infected with prions. *J. Biol. Chem.* **274**: 20763–20771.
  39. Kuziemko, G. M., M. Stroh, and R. C. Stevens. 1996. Cholera toxin binding affinity and specificity for gangliosides determined by surface plasmon resonance. *Biochemistry.* **35**: 6375–6384.
  40. Sharma, D. K., A. Choudhury, R. D. Singh, C. L. Wheatley, D. L. Marks, and R. E. Pagano. 2003. Glycosphingolipids internalized via caveolar-related endocytosis rapidly merge with the clathrin pathway in early endosomes and form microdomains for recycling. *J. Biol. Chem.* **278**: 7564–7572.
  41. Yamashiro, D. J., and F. R. Maxfield. 1984. Acidification of endocytic compartments and the intracellular pathways of ligands and receptors. *J. Cell. Biochem.* **26**: 231–246.
  42. Ichikawa, S., N. Nakajo, H. Sakiyama, and Y. Hirabayashi. 1994. A mouse B16 melanoma mutant deficient in glycolipids. *Proc. Natl. Acad. Sci. USA.* **91**: 2703–2707.
  43. Hammache, D., G. Pieroni, N. Yahi, O. Delezay, N. Koch, H. Lafont, C. Tamalet, and J. Fantini. 1998. Specific interaction of HIV-1 and HIV-2 surface envelope glycoproteins with monolayers of galactosylceramide and ganglioside GM3. *J. Biol. Chem.* **273**: 7967–7971.
  44. Seppo, A., M. Moreland, H. Schweingruber, and M. Tiemeyer. 2000. Zwitterionic and acidic glycosphingolipids of the *Drosophila melanogaster* embryo. *Eur. J. Biochem.* **267**: 3549–3558.
  45. Sharma, P., R. Varma, R. C. Sarasij, Ira, K. Gousset, G. Krishnamoorthy, M. Rao, and S. Mayor. 2004. Nanoscale organization of multiple GPI-anchored proteins in living cell membranes. *Cell.* **116**: 577–589.
  46. Kusumi, A., and K. Suzuki. 2005. Toward understanding the dynamics of membrane-raft-based molecular interactions. *Biochim. Biophys. Acta.* **1746**: 234–251.
  47. Orlandi, P. A., and P. H. Fishman. 1998. Filipin-dependent inhibition of cholera toxin: evidence for toxin internalization and activation through caveolae-like domains. *J. Cell Biol.* **141**: 905–915.
  48. Widengren, J., and P. Thyberg. 2005. FCS cell surface measurements—photophysical limitations and consequences on molecular ensembles with heterogenic mobilities. *Cytometry A.* **68**: 101–112.
  49. Simons, M., P. Keller, B. De Strooper, K. Beyreuther, C. G. Dotti, and K. Simons. 1998. Cholesterol depletion inhibits the generation of beta-amyloid in hippocampal neurons. *Proc. Natl. Acad. Sci. USA.* **95**: 6460–6464.
  50. Narayan, K., and M. A. Lemmon. 2006. Determining selectivity of phosphoinositide-binding domains. *Methods.* **39**: 122–133.